Supporting Information

An Octacarboxylate-Linked Sodium Metal-Organic Framework with High Porosity

Jiafeng Miao,[1] Wells Graham,[2] Jiaqi Liu,[1] Ena Clementine Hill,[2] Lu-Lu Ma,[1] Saif Ullah,[2] Hai-Lun Xia,[1] Fu-An Guo,[1] Timo Thonhauser,[2] Davide M. Proserpio,[3] Jing Li,[4,1] and Hao Wang[1]*

[1]Hoffmann Institute of Advanced Materials, Shenzhen Polytechnic University, 7098 Liuxian Boulevard, Shenzhen, Guangdong 518055, P. R. China.

[2]Department of Physics and Center for Functional Materials, Wake Forest University, Winston-Salem, NC 27109, United States.

[3]Dipartimento di Chimica, Università degli Studi di Milano, 20133 Milano, Italy.

[4]Department of Chemistry and Chemical Biology, Rutgers University, Piscataway, New Jersey 08854, United States.

Experimental details

Materials and characterizations. All reagents were obtained from commercial sources and used without further purification. Powder X-ray diffraction patterns were recorded on a Bruker D8 Advance with Cu Kα radiation (λ = 1.5406 Å). Data were collected at room temperature at 2θ = 3-40°. Thermogravimetric analysis was carried out on a TGA550 (TA Instruments) analyzer. For each run, 3-5 mg of sample was heated from room temperature to 600 °C at a ramp rate of 10 °C/min. Nitrogen adsorption at 77 K was measured on a BSD instrument automatic high performance surface area and aperture analyzer (BSD-660), and the sample was regenerated at 150 °C for 30 minutes. Single-crystal X-ray diffraction data were collected at 204 K on a Bruker APEX-II CCD diffractometer using GaKα radiation tuned to λ = 1.34139 Å. The structure was solved by direct methods and refined by full-matrix least-squares on F^2 using the Bruker SHELXTL package.

Synthesis of HIAM-111. NaCl (10 mg, 99.9% AR) and H_8ETTBPDC (30 mg, 98%) were added to a mixed solvent of DMF (99.9%, AR)/deionized water (10/1 mL), and the solution was transferred to a 20 mL glass bottle. The bottle was placed in an oven preset at 120 °C for 3 days and light yellow block-shaped crystals suitable for single-crystal X-ray diffraction analysis were harvested. The as synthesized HIAM-111 sample was exchanged with acetone and then evacuated under dynamic vacuum at 423 K for 12 h to obtain activated form of HIAM-111.

IAST selectivity calculation. The dual site Langmuir-Freundlich model was adopted to fit the adsorption isotherms of HIAM-111, which was described as follows:

$$q=q_{A,sat}\frac{b_A P^{v_A}}{1+b_A P^{v_A}}+q_{B,sat}\frac{b_B P^{v_B}}{1+b_B P^{v_B}}$$

with T-dependent parameters b_A, and b_B

$$b_A=b_{AO}\,exp\left(\frac{E_A}{RT}\right);\ b_B=b_{BO}\,exp\left(\frac{E_B}{RT}\right)$$

where q represents the adsorption amount of adsorbents with units of mol·kg^{-1}, $q_{A,sat}$ and $q_{B,sat}$ represent the saturated adsorption amount for adsorption sites A and B, respectively, b_A and b_B are constants for species i at adsorption sites A and B, respectively, p is the total pressure of the bulk gas at the adsorption equilibrium, and v_A and v_B are the Freundlich exponent for sites A and B, respectively.

Taking the C_2H_6/C_2H_4 selectivity as example, the IAST selectivity is defined by:

$$S_{ads}=\frac{q_1/q_2}{y_1/y_2}$$

where q_1 and q_2 represents the adsorption amounts of C_2H_6 and C_2H_4 under equilibrium condition, which are usually expressed with units of mmol·g^{-1}, y_1 and y_2 are the corresponding mole fractions in the gas phase for the mixtures. The calculated IAST adsorption selectivity for the C_2H_6/C_2H_4 (C_2H_6/C_2H_4 = 1/1; v/v) mixtures taking the mole fractions y_1 = 0.5 and y_2 = 1-y_1 = 0.5 for a total pressure of 101 kPa at 298 K.

Isosteric heat of adsorption. The adsorption heat of each component was determined precisely according to the virial fitting parameters of single-component adsorption isotherms measured at 278 K and 298 K up to 100 kPa.

Qst = -slope × R by drawing the Ln(P) *versus* gas uptakes, which was defined as follows:

$$Ln(P)=Ln(N)+\frac{1}{T}\sum_{i=0}^{m} a_i N_i+\sum_{i=0}^{n} b_i N_i$$

$$Q_{st}=-R\sum_{i=0}^{m} a_i N_i$$

where N is the adsorption amount, and m and n determine the number of items required to precisely fit the adsorption isotherms.

Multicomponent column breakthrough measurements. Breakthrough tests were carried out in an auto mixed-gas breakthrough apparatus (3P Mixsorb S). The mass of adsorbents filled into the column (I.D. 6 mm, length 100 mm) was 1.21 g. The adsorbents were activated at 423 K for 10 h under helium purging (10 ml/min) prior to the measurements. When the temperature was cooled down to 298 K, helium flow was stopped and the binary or ternary feed mixed gases at a flow rate of 1 mL/min were introduced to the adsorption column. The outlet gas was analyzed using an online mass spectrometer (MKS circus 3). After the adsorption reached dynamic equilibrium, the column was purged with helium (10 mL/min) at room temperature for 5 h for regeneration.

The purity (c) of the breakthrough gas was calculated by the following equation.

$$c = \frac{q_{C2H4}}{q_{C2H2}+q_{C2H4}+q_{C2H6}}$$

Computational calculations. Due to the large pore size of HIAM-111, we used classical grand canonical Monte Carlo (GCMC) simulations-with the help of the RASPA code[1]-to effectively sample the configurational space and find all binding locations. The HIAM-111 was treated as a rigid framework, and the DREIDING[2] model was adopted for force field parameters to represent the constituent atoms. For the guest molecules (CO_2, C_2H_2, C_2H_4, and C_2H_6), these reported parameters were used respectively[3-5].

The simulation is carried out at room temperature with a pressure of 1 bar. The cutoff distance for intermolecular interactions is set to 12 Å with the default Lorentz-Berthelot mixing rules. For the guest molecules with partial charges, we used the extended charge equilibration method to represent the framework charges[6]. Throughout the GCMC simulation, we recorded multiple configurations over 100,000 cycles. This enables us to visualize the binding location of guest molecules within the pore.

To study the molecular adsorption in HIAM-111 at the binding sites identified with our GCMC simulations, *ab initio* calculations were performed using the VASP code (version 6.4.0)[7-8]. To account for van der Waals interactions, we employ a vdW-DF3-opt1 functional[9] in conjunction with the standard PAW pseudopotentials[9]. The implementation of vdW-DF3-opt1 is previously discussed[10]. Gamma-point sampling is used due to the large MOF unit cell, consisting of 440 atoms and having lattice constants of a = 19.06, b = 31.86, and c = 14.52 Å. The kinetic energy cutoff is set to 520 eV to ensure converged results. For geometric optimization, we set the criteria at 10^{-6} eV for the self-consistent field (SCF) loop and 0.005 eV $Å^{-1}$ for forces. To quantify the binding strength, we calculated the energy difference between the loaded

MOF and the sum of the energies of the individual empty MOF and the gas-phase guest molecules using the following equation:

$$E_b = E_{MOF} + E_{guest} - E_{loaded}$$

Here, E_{loaded} represents the MOF loaded with a specific guest molecule, E_{MOF} stands for the energy of the empty framework, and E_{guest} is the energy of the isolated guest molecule.

1. Dubbeldam, D.; Calero, S.; Ellis, D. E.; Snurr, R. Q., RASPA: molecular simulation software for adsorption and diffusion in flexible nanoporous materials. Molecular Simulation 2016, 42 (2), 81-101.

2. Mayo, S. L.; Olafson, B. D.; Goddard, W. A., DREIDING: a generic force field for molecular simulations. The Journal of Physical Chemistry 1990, 94 (26), 8897-8909.

3. Potoff, J. J.; Siepmann, J. I., Vapor–liquid equilibria of mixtures containing alkanes, carbon dioxide, and nitrogen. AIChE Journal 2001, 47 (7), 1676-1682.

4. Liu, B.; Smit, B.; Rey, F.; Valencia, S.; Calero, S., A New United Atom Force Field for Adsorption of Alkenes in Zeolites. The Journal of Physical Chemistry C 2008, 112 (7), 2492-2498.

5. Boyd, P. G.; Moosavi, S. M.; Witman, M.; Smit, B., Force-Field Prediction of Materials Properties in Metal-Organic Frameworks. The Journal of Physical Chemistry Letters 2017, 8 (2), 357-363.

6. Wilmer, C. E.; Kim, K. C.; Snurr, R. Q., An Extended Charge Equilibration Method. The Journal of Physical Chemistry Letters 2012, 3 (17), 2506-2511.

7. Kresse, G.; Furthmüller, J., Efficient iterative schemes for ab initio total-energy calculations using a plane-wave basis set. Physical Review B 1996, 54 (16), 11169-11186.

8. Kresse, G.; Joubert, D., From ultrasoft pseudopotentials to the projector augmented-wave method. Physical Review B 1999, 59 (3), 1758-1775.

9. Chakraborty, D.; Berland, K.; Thonhauser, T., Next-Generation Nonlocal van der Waals Density Functional. Journal of Chemical Theory and Computation 2020, 16 (9), 5893-5911.

10. Ullah, S.; Jensen, S.; Liu, Y.; Tan, K.; Drake, H.; Zhang, G.; Huang, J.; Klimeš, J.; Driscoll, D. M.; Hermann, R. P.; Zhou, H.-C.; Li, J.; Thonhauser, T., Magnetically Induced Binary Ferrocene with Oxidized Iron. Journal of the American Chemical Society 2023, 145 (32), 18029-18035.

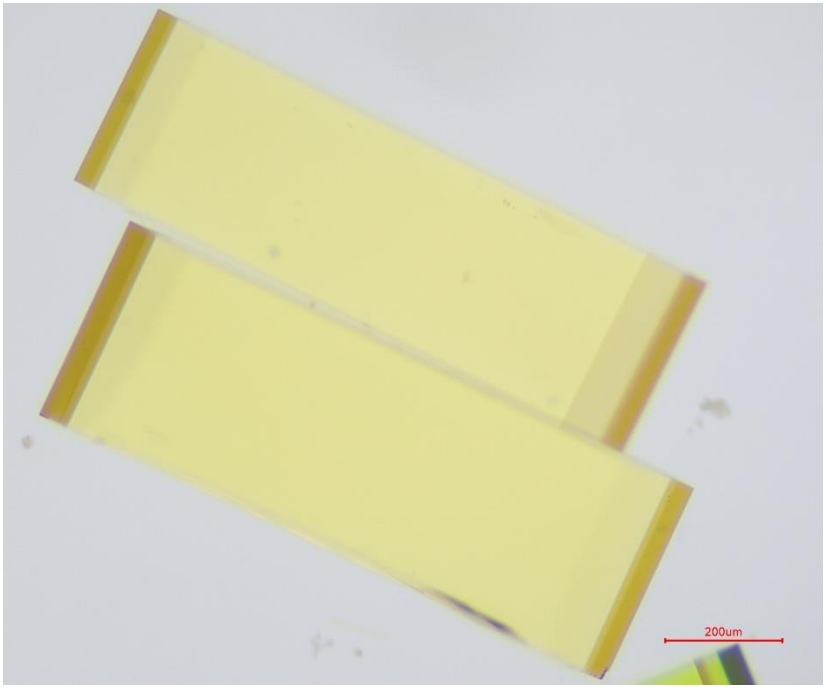

Figure S1. Optical image of the as-synthesized HIAM-111 crystals.

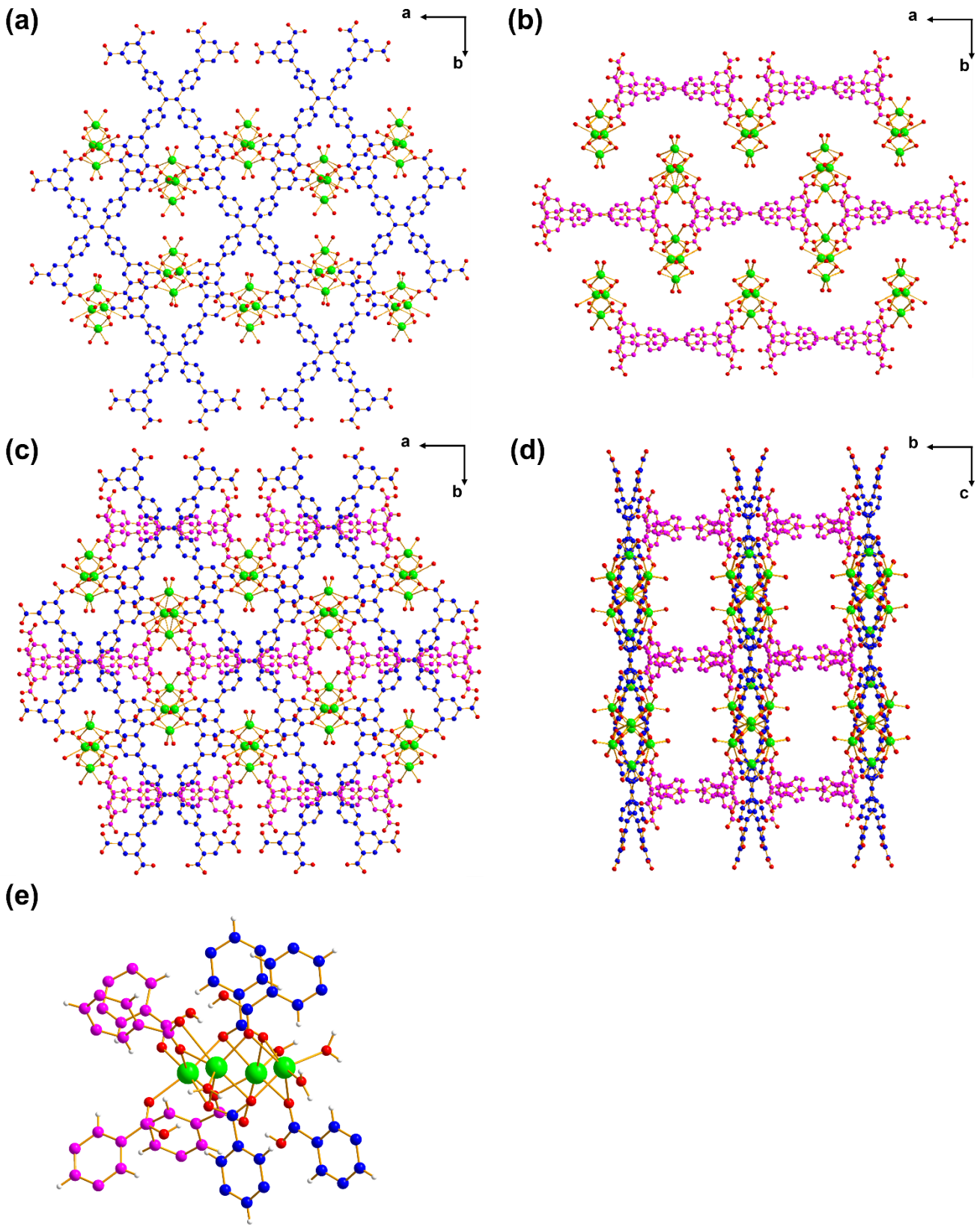

Figure S2. 8-connected Na_4 clusters in the crystal structure of HIAM-111. Blue and pink colored linkers represent octacarboxylates in different mode.

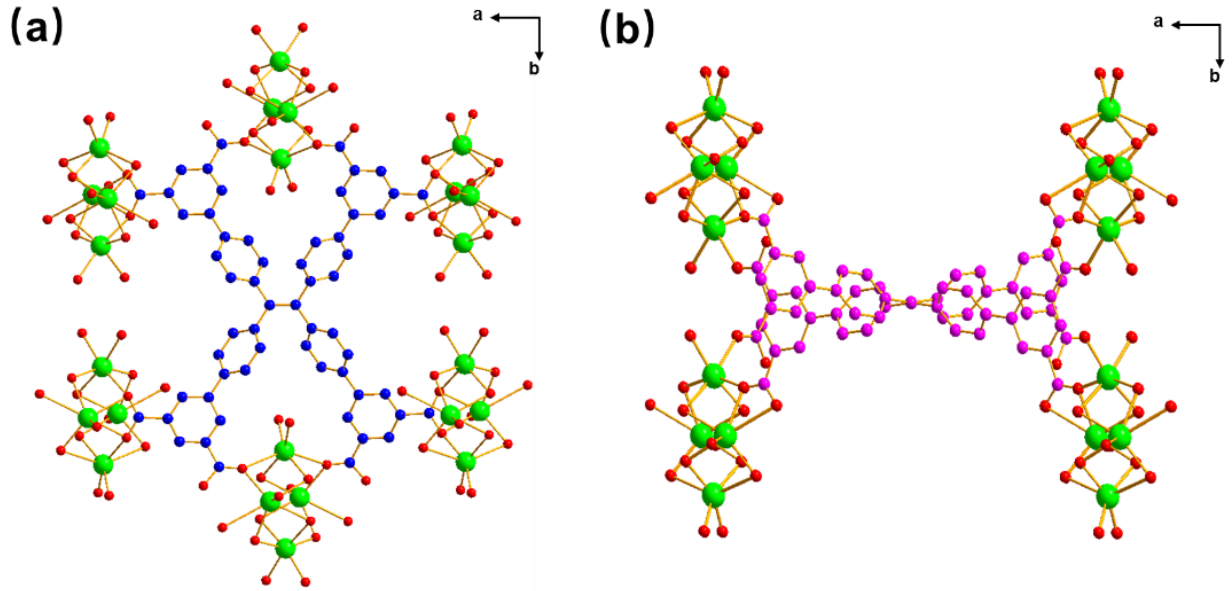

Figure S3. Two different modes of the organic linker (marked in different colors) in the crystal structure of HIAM-111.

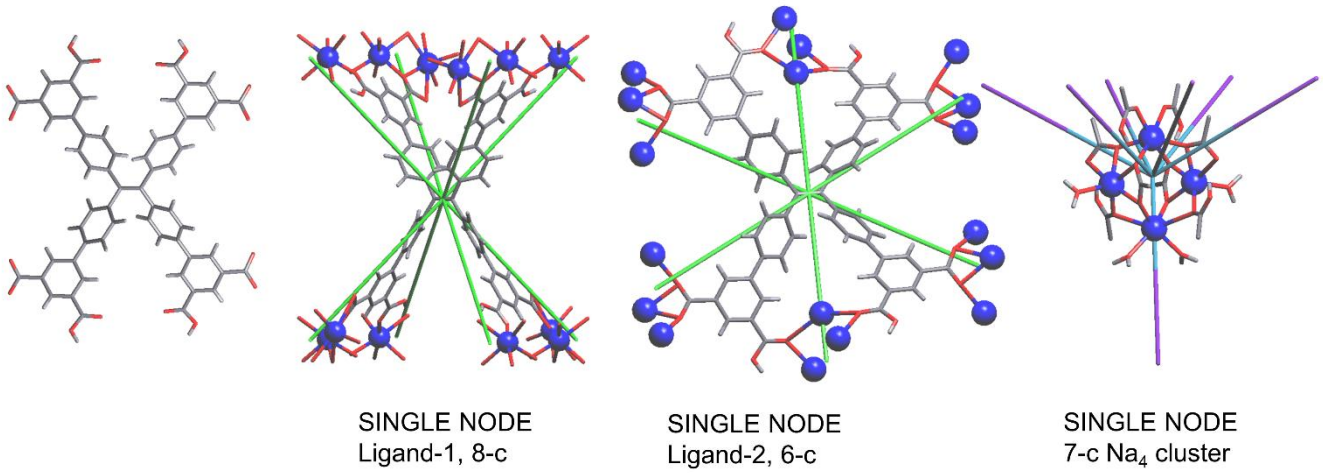

Figure S4. Topology analysis of HIAM-111 in single node description resulting in a new net named *hia*3 6,7,8-c trinodal net with 6-c and 8-c for the two distinct ligands and 7-c for the Na cluster. Point symbol $\{4^{10}\cdot6^{4}\cdot8\}\{4^{17}\cdot6^{4}\}_2\{4^{20}\cdot6^{8}\}$.

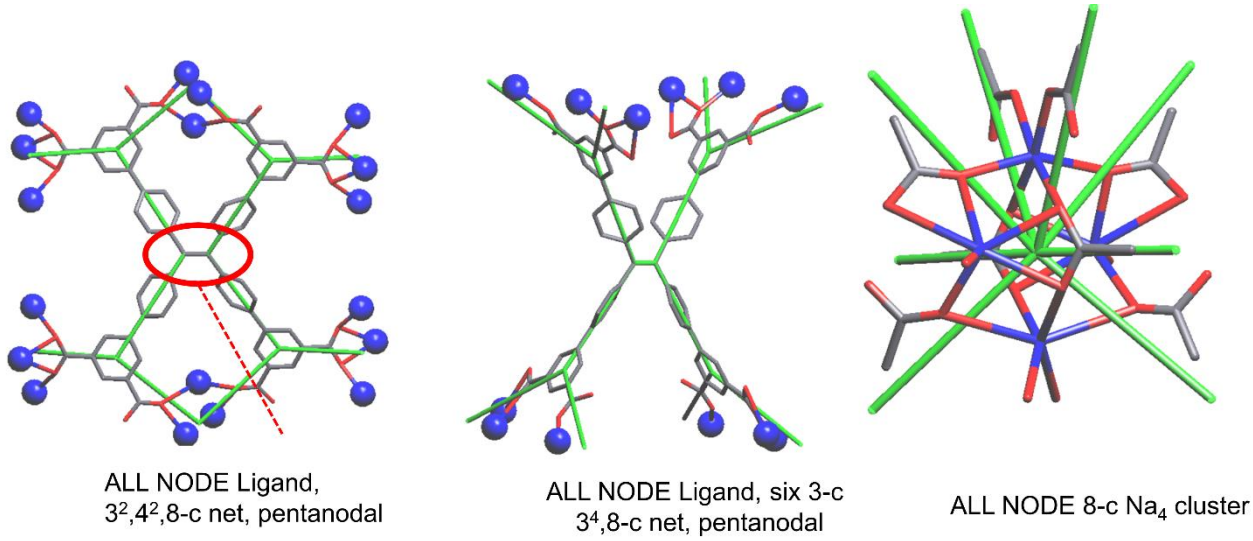

Figure S5. Topology analysis of HIAM-111 in the two possible all node cluster descriptions. The Na_4 SBU is always 8-c while the ligands may be represented in two different ways, as shown from the left, with a 4-c node representing the central C=C and four 3-c nodes, or (center) with six 3-c nodes mapping all the ramifications of the ligand. The two representations result in two new distinct underlying nets named *hia*2 for the pentanodal $3^2,4^2$,8-c net (Point Symbol $\{4\cdot8^2\}_4\{4^2\cdot6\}_4\{8^4\cdot12^2\}\{4^2\cdot6^2\cdot8^2\}\{4^9\cdot6^{10}\cdot8^9\}_2$). and *hia*1 for the 3^4,8-c (Point Symbol $\{4\cdot8^2\}_2\{4\cdot5\cdot6\}_2\{8\cdot10^2\}\{5^2\cdot6\}\{4^8\cdot5\cdot6^8\cdot7^2\cdot8^9\}$).

The coordinates of the 3 nets *hia*1, *hia*2, *hia*3 are available as supplementary cif files (with the connectivity according to the latest Topocif dictionary)[1] and have been deposited in the personal.ttd database included in the TopCryst system.[2]

1 www.iucr.org/resources/cif/dictionaries/cif_topology

2 A. P. Shevchenko, A. A. Shabalin, I. Y. Karpukhin and V. A. Blatov, Topological representations of crystal structures: generation, analysis and implementation in the TopCryst system, Sci. Technol. Adv. Mater.: Methods, 2022, 2, 250-265. http://topcryst.com

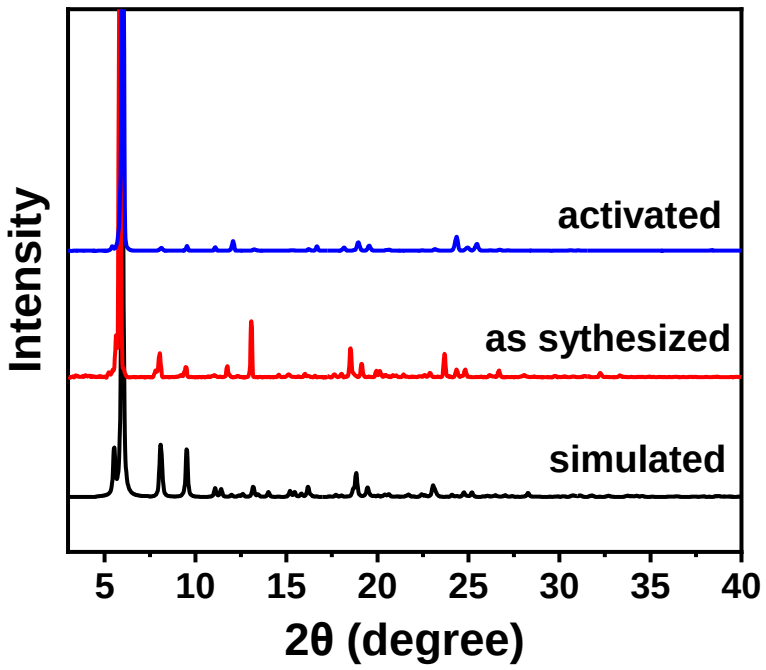

Figure S6. PXRD patterns of the activated and as-synthesized HIAM-111 samples compared to the simulated one.

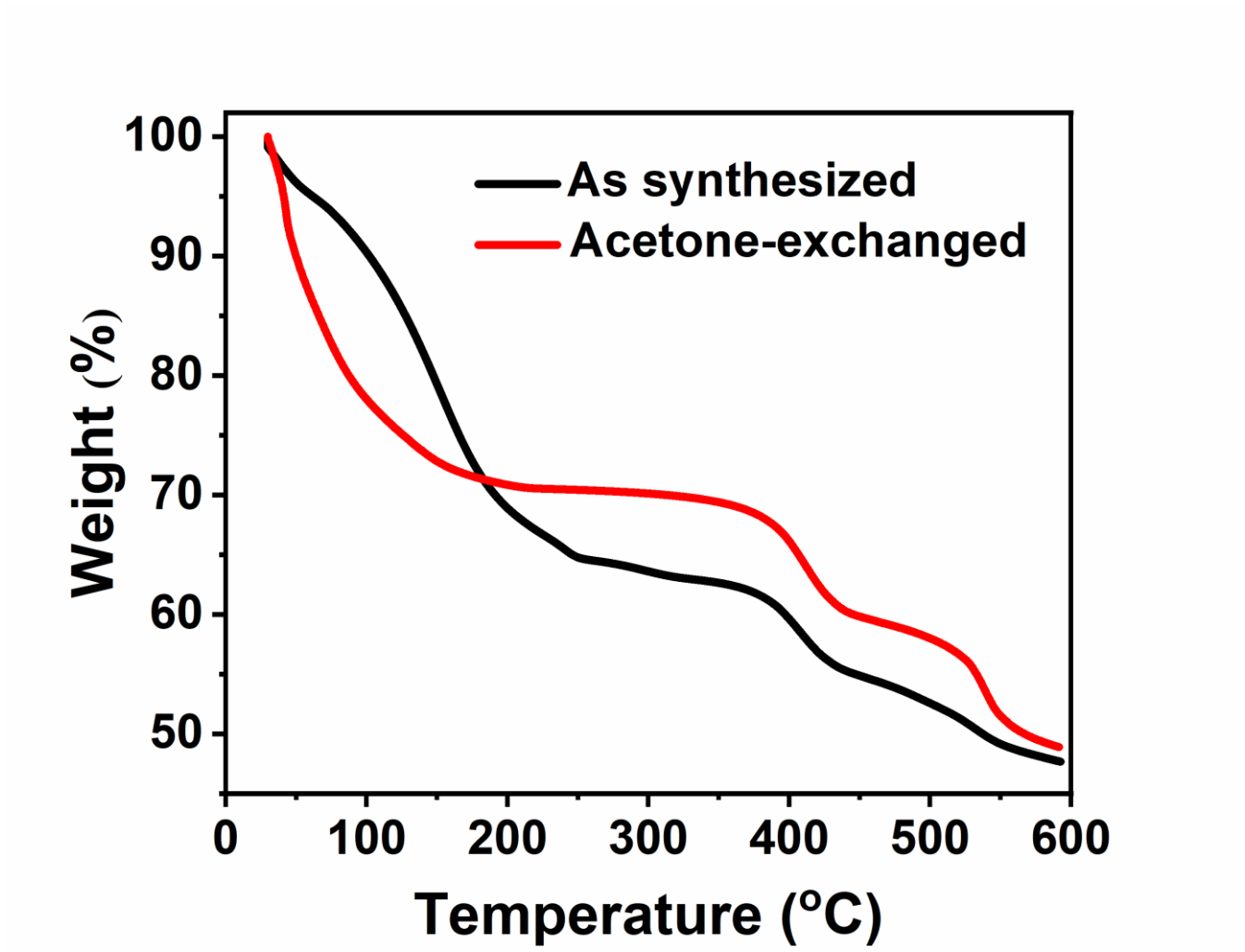

Figure S7. TG curves of the as synthesized and acetone-exchanged HIAM-111 samples.

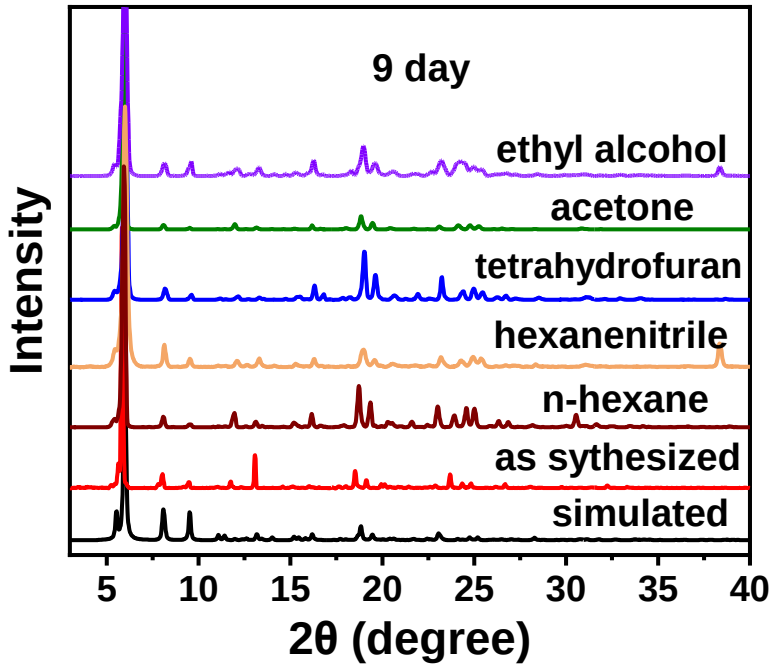

Figure S8. PXRD patterns of the HIAM-111 samples after being soaked in different solvents for 9 days.

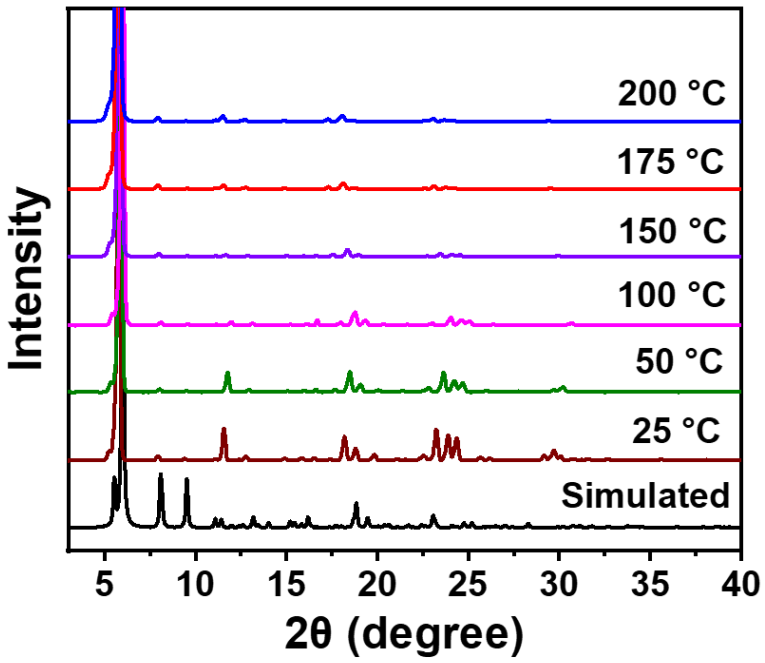

Figure S9. PXRD patterns of the HIAM-111 sample collected at various temperatures compared with the simulated one.

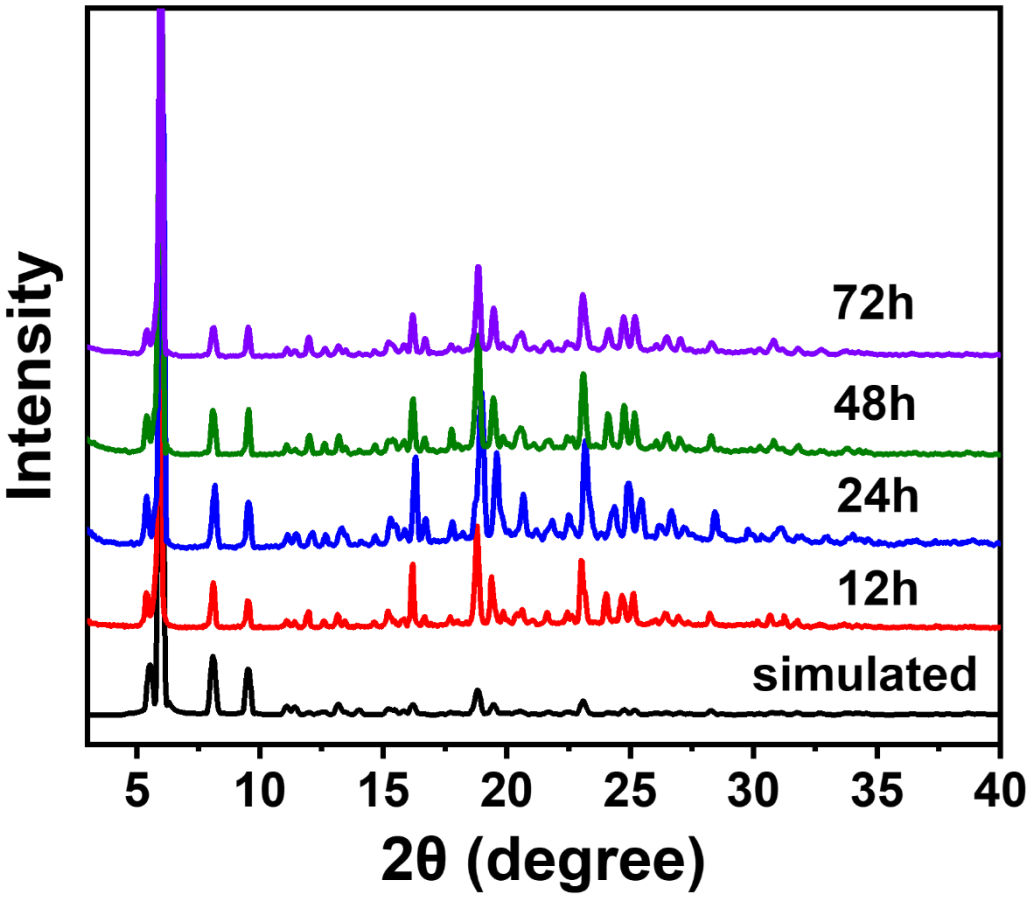

Figure S10. PXRD patterns of the HIAM-111 sample upon exposure in air (70-80%RH).

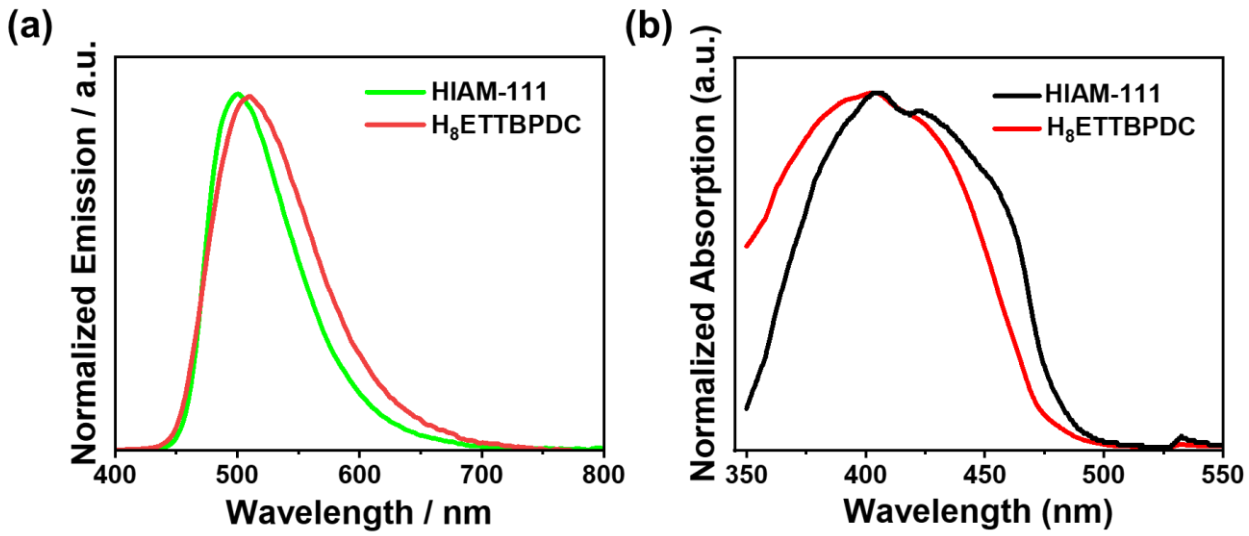

Figure S11. (a) Fluorescent spectra of HIAM-111 and H_8ETTBPDC at room temperature excited at 360 nm, (b) Solid state diffuse reflectance spectra of HIAM-111 and H_8ETTBPDC.

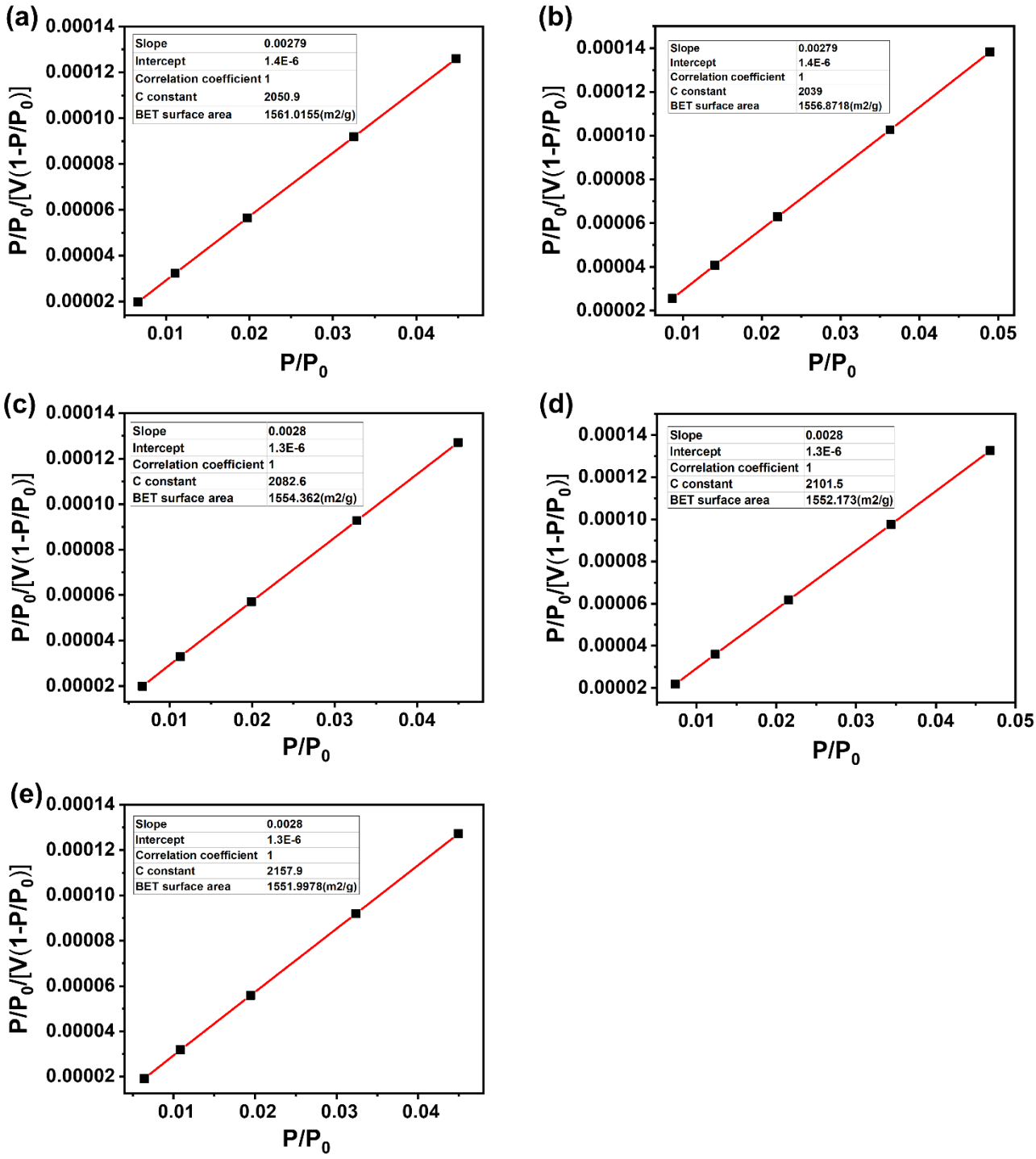

Figure S12. BET plots of the five consecutive N_2 adsorption isotherms at 77 K.

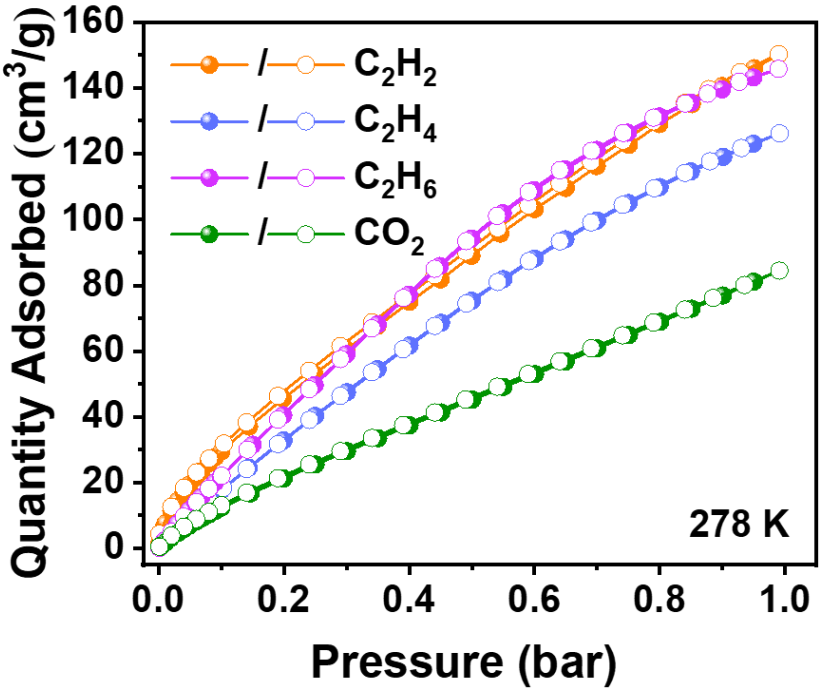

Figure S13. C_2H_2, C_2H_4, C_2H_6, and CO_2 adsorption-desorption isotherms on HIAM-111 at 278 K.

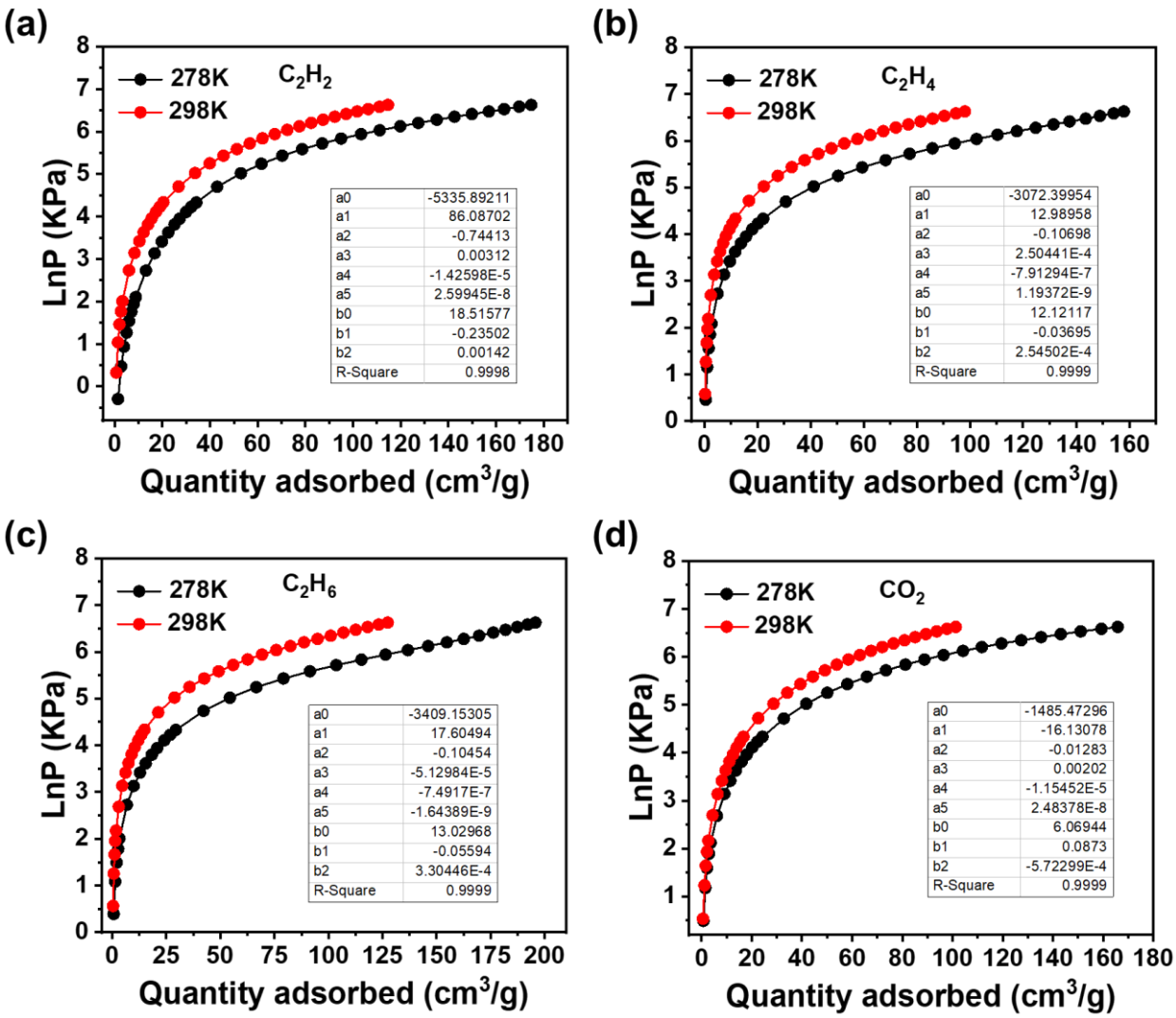

Figure S14. The fitting curves and parameters of Viral equation for adsorption isotherms of C_2H_2, C_2H_4, C_2H_6, and CO_2 on HIAM-111.

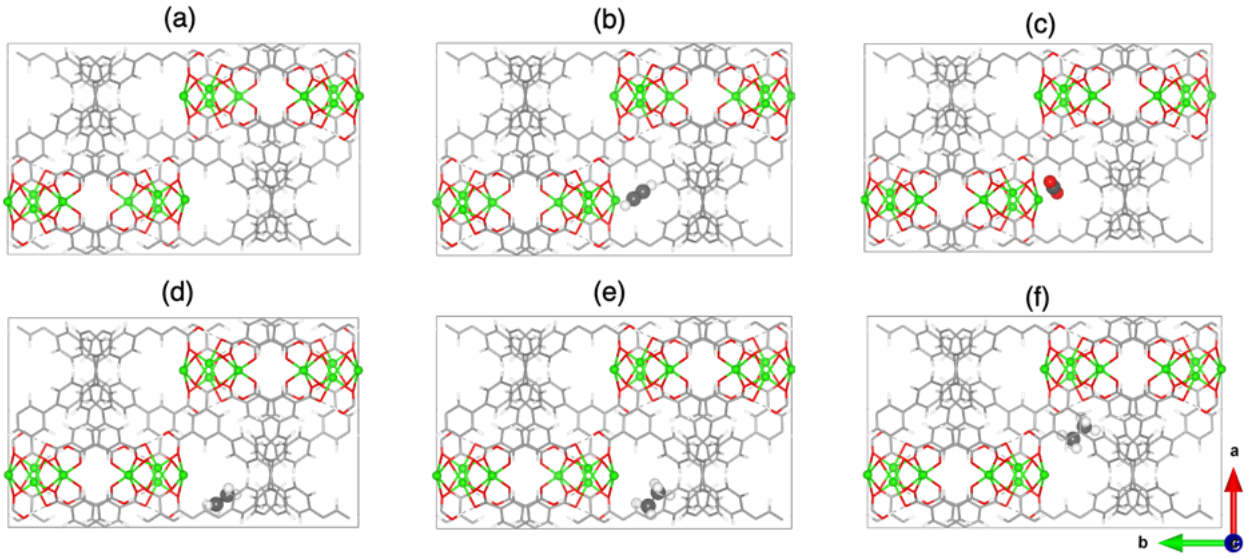

Figure S15. vdW-DF3-opt1 optimized structures of (a) activated MOF, (b) C_2H_2 loaded, (c) CO_2 loaded, (d) C_2H_4 loaded, (e) C_2H_6 loaded at optimum binding sites. Panel (f) shows secondary binding site for C_2H_6.

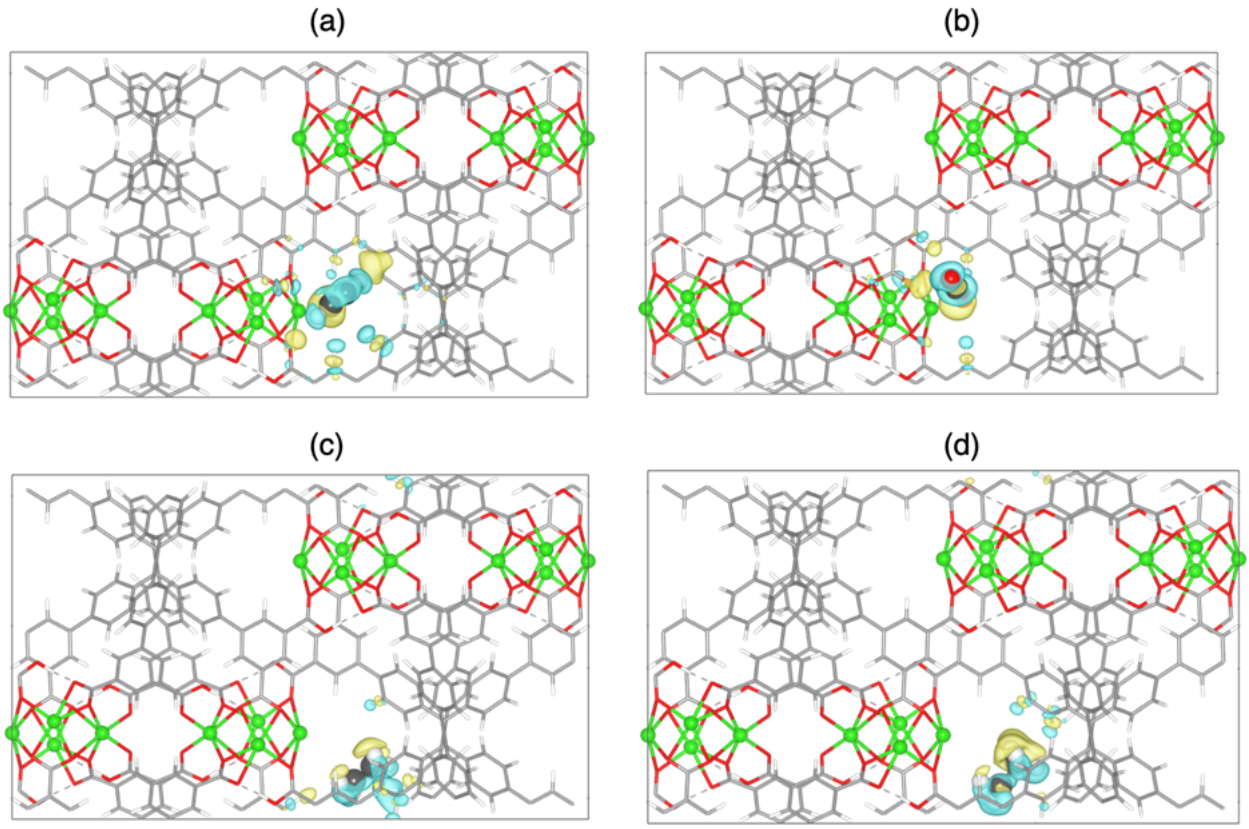

Figure S16. Induced charge densities of (a) C_2H_2@MOF (b) CO_2@MOF, (c) C_2H_4@MOF, and (d)C_2H_6@MOF.

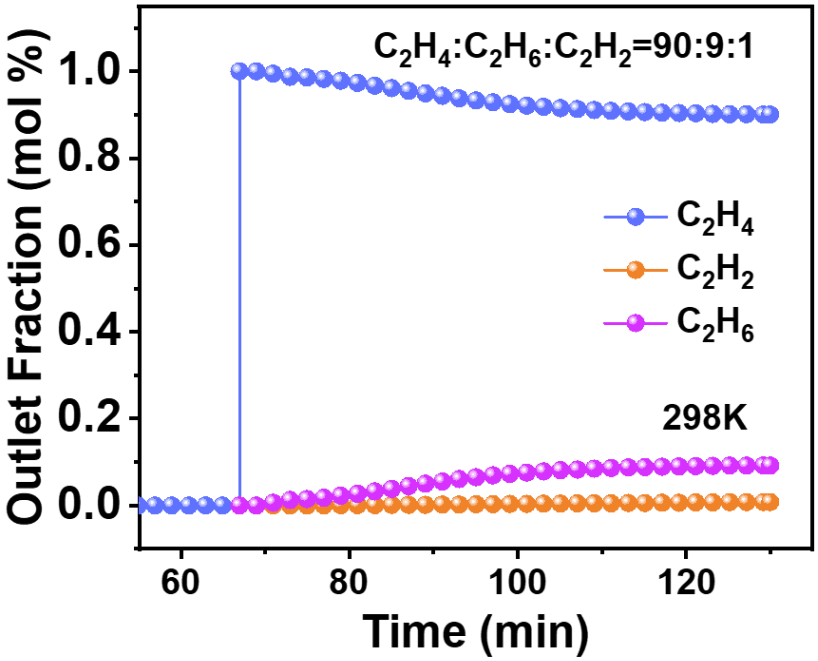

Figure S17. Breakthrough curves of a ternary mixture of $C_2H_2/C_2H_4/C_2H_6$ (1/90/9) on HIAM-111 at 298 K.

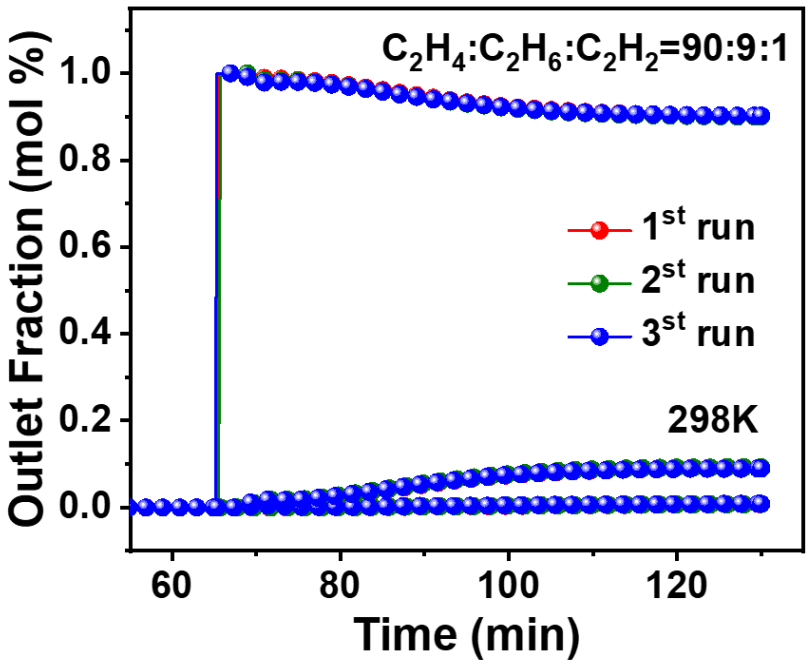

Figure S18. Three consecutive breakthrough curves of a ternary mixture $C_2H_2/C_2H_4/C_2H_6$ (1/90/9) on HIAM-111 at 298 K (99.5% Ethylene productivity: 0.0248 L/kg).

Table S1. Crystal data and structure refinement parameters for the as synthesized HIAM-111.

Empirical formula	C58 H38 Na4 O19
Formula weight	1130.84
Temperature/K	204
Crystal system	Orthorhombic
Space group	Pban
a/Å	19.057(3)
b/Å	31.856(4)
c/Å	14.5183(19)
α/°	90
β/°	90
γ/°	90
Volume/Å3	8814(2)
Z	4
ρcalcg/cm3	0.852
μ/mm-1	0.451
F(000)	2328.0
Crystal size/mm3	0.13 x 0.12 x 0.1
Radiation	GaKα (λ = 1.34139)
2Θ range for data collection/°	4.7 to 107.804°
Index ranges	-22<=h<=22, -38<=k<=35, -15<=l<=17
Reflections collected	41467
Independent reflections	8074 [R(int) = 0.1046]
Data/restraints/parameters	8074 / 0 / 376
Goodness-of-fit on F2	0.999
Final R indexes [I>=2σ (I)]	R1 = 0.0919, wR2 = 0.2748
Final R indexes [all data]	R1 = 0.1456, wR2 = 0.3215
Largest diff. peak/hole / e Å-3	1.10/-0.40

Table S2. Fitting parameters of Dual-site Langmuir-Freundlich isotherm model.

	CO_2	C_2H_2	C_2H_4	C_2H_6
a0	140.48141	209.25813	1.86843	1.66164
b1	3.93595E-4	6.81264E-4	1.91261E-4	1.06645E-5
c1	0.74704	0.73378	1.59147	2.51172
a2	81.10222	0.95782	27.39291	10.82097
b2	8.29143E-5	5.75837E-6	0.00169	0.00487
c2	0.97013	2.44014	0.93692	0.98248
Chi^2	2.60732E-5	6.09919E-5	8.97235E-6	2.05516E-6
R^2	0.9999	0.9999	0.9999	0.9999